

Compact Rotman Lens Structure Configurations to Support Millimeter Wave Devices

Toan K. Vo Dai* and Ozlem Kilic

Abstract—The development of modern communication devices for the latest technologies such as 5G has brought the millimeter wave technology into the spotlight because it offers higher data rates and bandwidth. Since highly directional transmissions are necessary for communication in these frequencies due to high path loss and atmospheric absorption, the use of adaptive antennas is inevitable. Rotman lenses have long been used as analog beam forming networks to support linear array antennas for electronic scanning. Their broad bandwidth and planar structure make them ideal for a variety of applications. However, their overall dimensions can be prohibitive especially for large scan angles. In this paper, we propose a few compact configurations that reduce the overall dimensions of Rotman lens as much as 50% without degrading its performance.

1. INTRODUCTION

Rotman lens, which was invented by Rotman and Tuner in 1962 [1], is a multiple input and multiple output analog beam former that creates a specific phase taper at the output ports to feed a linear array antenna. In the past few decades, methods to improve the magnitude and phase performance of Rotman lenses have been considered for the conventional lens equations [2–8] or using optimization methods [9–11]. These lenses can be used for many applications such as multi-beam wireless communication systems in military [12–15]. With the development of fabrication technologies, numerous Rotman lens designs have been developed employing different techniques including microstrip [2, 5–8], graded dielectric substrates [16] or substrate integrated waveguides [17–24]. However, these designs still have a planar structure with a large electrical size which makes it difficult to integrate them into modern devices such as smart watches, mobile phones, curved TVs, or GPS devices, etc. There have been some solutions that propose the design of a compact dual-layer Rotman lens [24] or folding the parallel-plate region of the Rotman lens along its middle plane and the two layers are interconnected through a wide strip-line transition [25]. In this paper, we modify the conventional Rotman lens structure to reduce overall dimensions based on the configurations of different platforms and compare their performances with the conventional lens. We employ the commercial software package FEKO to study the performance characteristics.

The remainder of the paper is organized as follows. Section 2 discusses the design procedure and simulation results of a conformal lens. Section 3 proposes a new design of folded lens while a wrapped lens concept is introduced in Section 4. Performances are compared with the conventional lens for each design. Conclusions are presented in Section 5. All these configurations reduce the overall dimensions while adapting to the natural environment for operation without sacrificing performance.

Received 27 August 2016, Accepted 7 November 2016, Scheduled 23 November 2016

* Corresponding author: Toan Khanh Vo Dai (30vodai@cua.edu).

The authors are with The Catholic University of America, Washington, DC 20064, USA.

2. CONFORMAL ROTMAN LENS ON SINGLY CURVED SURFACES

The objective of the conformal configuration in this paper is to integrate the Rotman lens onto singly curved surfaces such as parabolic, elliptical or cylindrical. Such a lens can be integrated on electronic devices such as curved TV, watch bands, or on the body of airplanes, high-speed trains, or other vehicles for multi-beam wireless communication purposes. We consider applications where the lens is curved across its dummy ports over the singly curved surface. This enables the input and output ports as well as the array antenna, which extend in the transverse direction to reside on the curvature of the surface. Since the overall dimensions of the array are small, the effects of the bend in the antenna structure have little or no effect on its radiation performance. Otherwise the curvature effects would need to be included for the array performance design as well as the lens design [11].

Figure 1(a) shows an example of the conformal lens system integrated on the back of a curved TV. Fig. 1(b) shows the conformal array structure we use as described above. As described above, due to its small dimensions (shown in Table 1), the conformal array structure can be considered having similar configuration with the planar array structure shown in Fig. 1(c). Therefore, it will be shown in the next section that the conformal array in Fig. 1(b) produces similar radiation pattern with the planar array in Fig. 1(c).

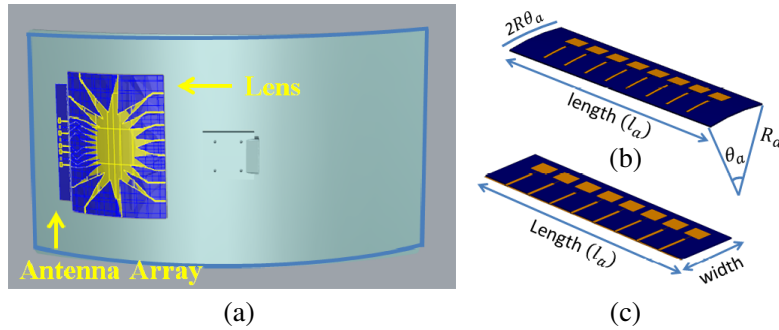


Figure 1. (a) Conformal lens system integrated on the back of a curved TV, (b) conformal array structure, and (c) planar array structure.

2.1. Design Procedure for Conformal Lens

In this section, we model the structure of the conformal lens using the commercial software package FEKO and analyze its performance. A challenge in modeling the conformal lens is to make sure the true-time delay properties of the new structure are the same with those of the original lens. Our conformal lens design is based on the original design of conventional Rotman lens and can be applied to different types of singly curved surfaces such as parabolic, cylindrical or elliptical. For simplicity, we focus on the cylindrical surface for this paper. Fig. 2(b) demonstrates the procedure to conform a conventional Rotman lens (as depicted in Fig. 2(a)) on a cylindrical surface defined by radius R .

The procedure to conform the lens on cylindrical surfaces is divided into two steps. The first step is to project all controlled points on the lens region, such as points A and B of the conventional lens as shown in Fig. 2(a), onto the cylindrical surface shown in Fig. 2(b). This can be done by applying Equation (1) to find the coordinates of the projected points A_p , B_p corresponding to the global coordinate as shown in Fig. 2(b).

$$x_{A_p} = R \cos \left(\frac{\frac{\pi R}{2} - |x_A|}{R} \right), \quad y_{A_p} = y_A, \quad z_{A_p} = R \sin \left(\frac{\frac{\pi R}{2} - |x_A|}{R} \right) - R \quad (1)$$

The second step is to plot the projected contour of the line (AB) between these two points (A_p , B_p) on the cylindrical surface by applying the geodesics equation on singly curved surfaces. The general

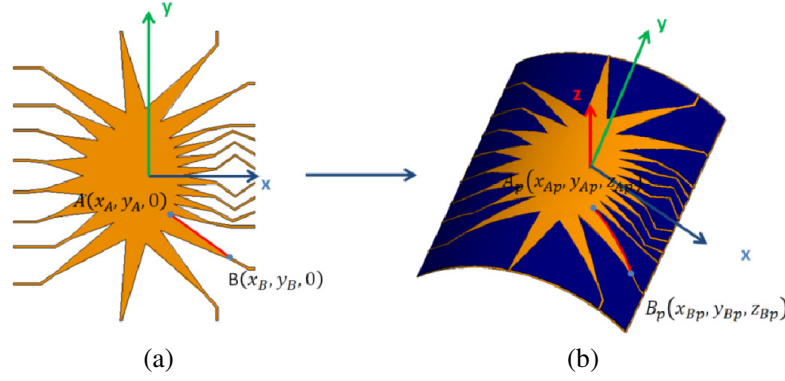


Figure 2. Design of conformal lens. (a) Conventional lens. (b) Conformal lens for cylindrical surface with radius R .

expression for a singly curved surface in the geodesics coordinate system [27, 28] is described as follows:

$$x = f(u), \quad y = g(u), \quad z = v \quad (2)$$

The geodesics equation for this singly curved surface becomes

$$\frac{dv}{du} = \frac{\pm \alpha \sqrt{(f'(u))^2 + (g'(u))^2}}{\sqrt{1 - \alpha^2}} \quad (3)$$

with the solution

$$v(u) = \frac{\pm \alpha}{\sqrt{1 - \alpha^2}} \int \sqrt{(f'(u))^2 + (g'(u))^2} du + \beta = \zeta(u, \alpha) + \beta \quad (4)$$

where α, β are geodesic constants and they can be calculated as provided in Eqs. (5) and (6).

$$v_{start} = \zeta(u_{start}, \alpha) + \beta \quad (5)$$

$$v_{stop} = \zeta(u_{stop}, \alpha) + \beta \quad (6)$$

For a cylindrical surface, Equation (2) becomes

$$x = f(u) = R \cos(\phi), \quad y = g(u) = R \sin(\phi), \quad z = z \quad (7)$$

where $u = \phi$ and $v = z$ in the global cylindrical coordinates.

From Eqs. (4)–(6), the geodesics equation for the cylindrical surface between two arbitrary points is calculated as:

$$z = \frac{\alpha}{\sqrt{1 - \alpha^2}} R \phi + \beta \quad (8)$$

Using Eq. (8), all contours in the conformal lens can be generated so that its true time delay properties are the same as the conventional lens. It should be noted that since the geodesics equation is applied on its local coordinates, i.e., cylindrical coordinate system for a cylindrical surface, in the second step to conform the lens, we apply (8) in the local geodesics coordinates of the surface. In this case, this local coordinate system has its origin at $O_{local}(0, 0, -R)$, and its unit vectors are $\vec{x}_{loc} = \vec{x}$, $\vec{y}_{loc} = -\vec{z}$, and $\vec{z}_{loc} = \vec{y}$.

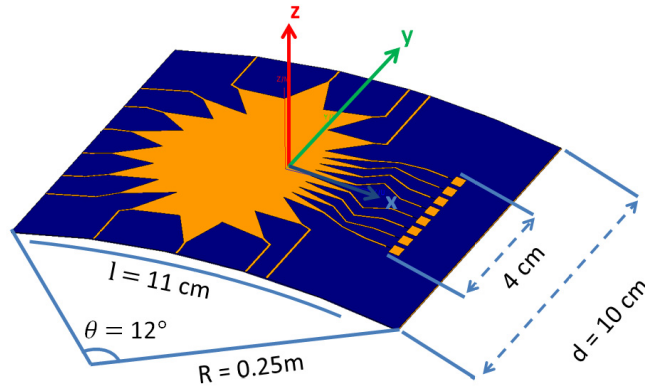
2.2. Simulation Results for Conformal Lens

To verify the robustness of our conformal lens design and analyze the effect of the radius of the conformed surface on the lens performance, we design two conformal lenses operating at a center frequency of 28 GHz and residing on the cylindrical surface with parameters specified as in Table 1. Case 2 represents a sharper curvature (defined by its radius R , width d and opening angle θ) compared to case 1, with all other parameters being identical. Commercial software package FEKO is employed to analyze the performance in each case. The results are presented and discussed below.

Table 1. Design parameters of conformal lens and conformal array.

Design parameters	Case 1	Case 2
Surface radius (R)	25 cm	15 cm
Width (d)	10 cm	10 cm
Subtended angle (θ)	20.5°	34.2°
Length ($l = 2\theta R$)	11 cm	11 cm
Center frequency (f_0)	28 GHz	28 GHz
Ultralam 3850 (ϵ_r)	2.9	2.9
Substrate Thickness (h)	0.25 mm	0.25 mm
Scanning range	-30° to 30°	-30° to 30°
Number of input	6	6
Number of output	8	8
Length of array antenna (l_a)	4 cm	4 cm
Subtended angle of array (θ_a)	2.8°	4.2°

Figure 3 shows the CAD model of the integrated system of the lens and the array on the conformal surface for case 1. Its magnitude and phase performance over the bandwidth from 26 GHz to 30 GHz is shown in Fig. 4 and Fig. 5, respectively. The performance of the planar conventional lens at the center frequency (i.e., 28 GHz) with identical design parameters is also plotted in Fig. 4 and Fig. 5 for a comparison. Fig. 6(a) shows the radiation pattern of the linear array on the planar structure (shown in Fig. 1(c)) fed by the output ports of the conventional planar lens while Fig. 6(b) shows the radiation pattern of the conformal array (shown in Fig. 1(b)) fed by the output ports of the conformal lens on the cylindrical surface in case 1. As mentioned above, it should be noted that the conformal array, which extends in the transverse direction to the curved surface, can be approximated as a linear array. This explains the similarity of radiation pattern in Fig. 6(a) and 6b of these two array antennas.

**Figure 3.** Design of the conformal lens for case 1.

We see from Fig. 4 and Fig. 5 that the amplitude and phase performances of the conformal lens in case 1 agree well with the conventional lens. The radiation pattern of the conformal array fed by this lens also has good performance with gain value at 10 dB and side lobe levels at about -2 dB.

The design of the conformal lens integrated with the conformal array for case 2 is shown in Fig. 7. Its magnitude and phase performances over a bandwidth from 26 GHz to 30 GHz are shown in Fig. 8 and Fig. 9, respectively. As before its performance is compared with the conventional lens designed using the same parameters. Fig. 10(a) shows the radiation pattern of the linear array on the planar structure (shown in Fig. 1(c)) fed by the output ports of the conventional planar lens while Fig. 6(b)

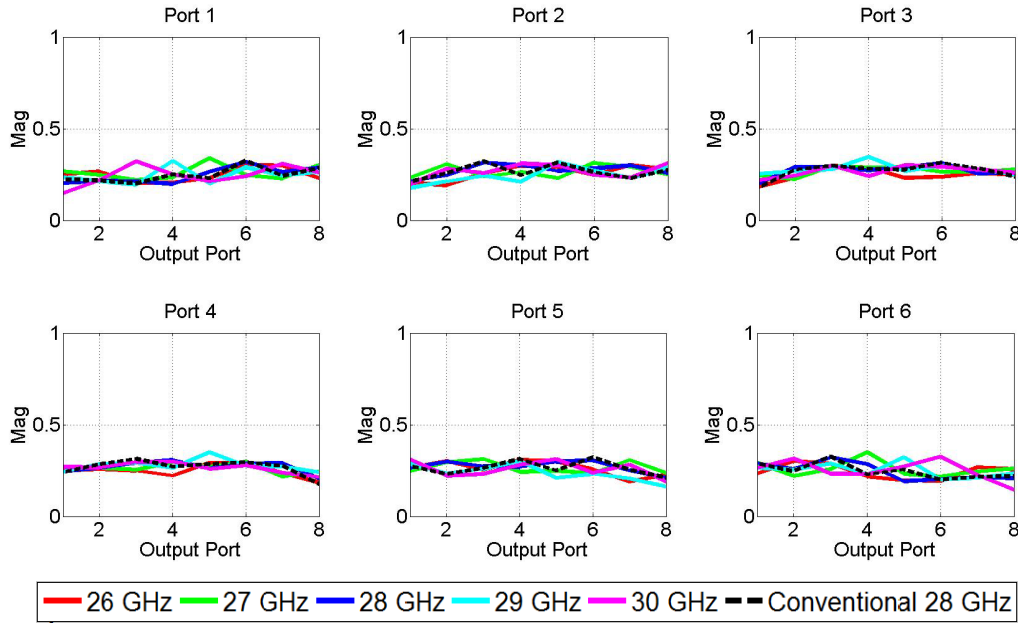


Figure 4. Magnitude performance of the conformal lens for case 1.

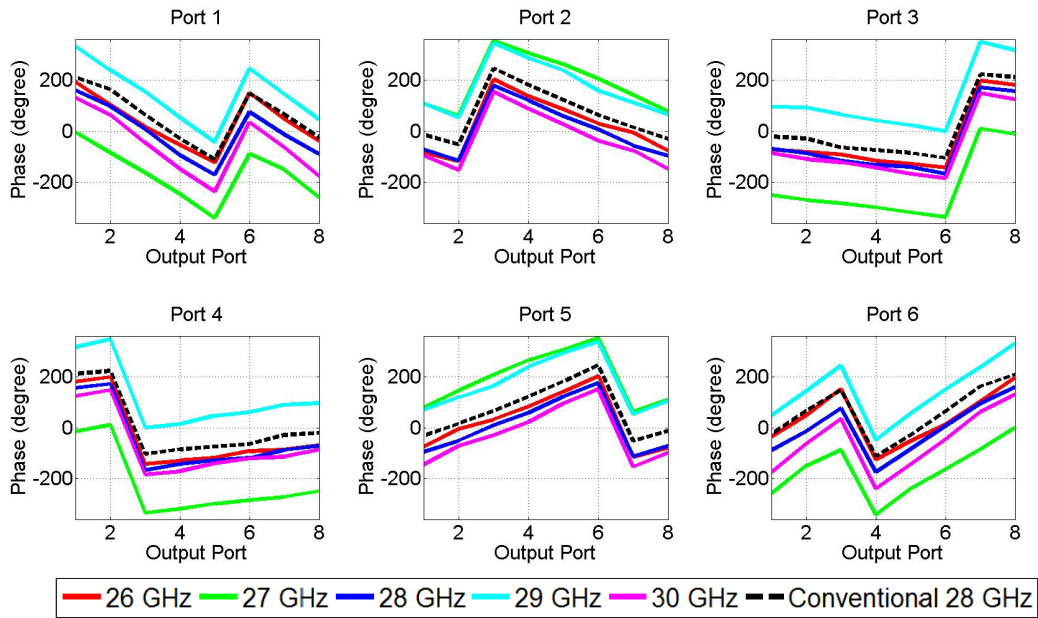


Figure 5. Phase performance of the conformal lens for case 1.

shows the radiation pattern of the conformal array (shown in Fig. 1(b)) fed by the output ports of the conformal lens on the cylindrical surface in case 2.

We see that although the conformal lens for Case 1 performs well compared with the conventional lens, the conformal lens for Case 2 suffers in its performance. The magnitudes of received voltage for Case 2 are attenuated by 10 dB more than those of Case 1, as depicted in Fig. 8. This is due to the fact that with a high degree curvature, the feed line structures of the lens are deformed significantly such that reflection coefficients produced when the wave goes around the circular structure becomes more significant. It is this increase in reflection coefficients that affects the phase performance of the lens as well as its magnitude performance. As can be shown in [29], these reflection coefficients vary inversely

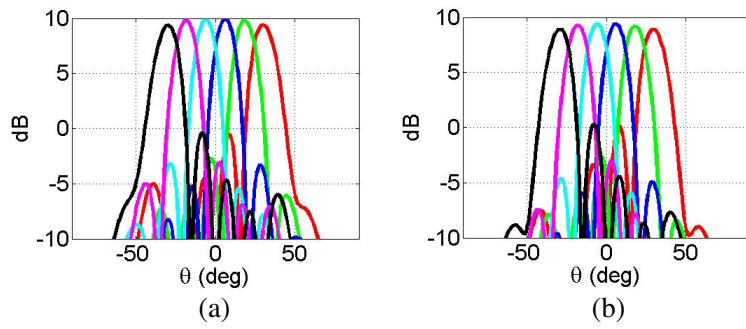


Figure 6. Radiation pattern of the (a) planar array, (b) conformal array fed by the lens in case 1 at 28 GHz.

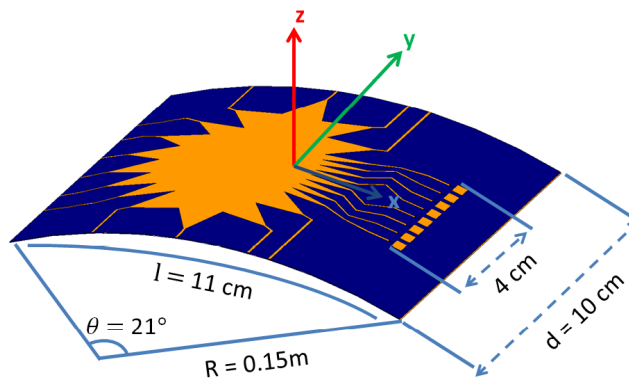


Figure 7. Design of the conformal lens for case 2.

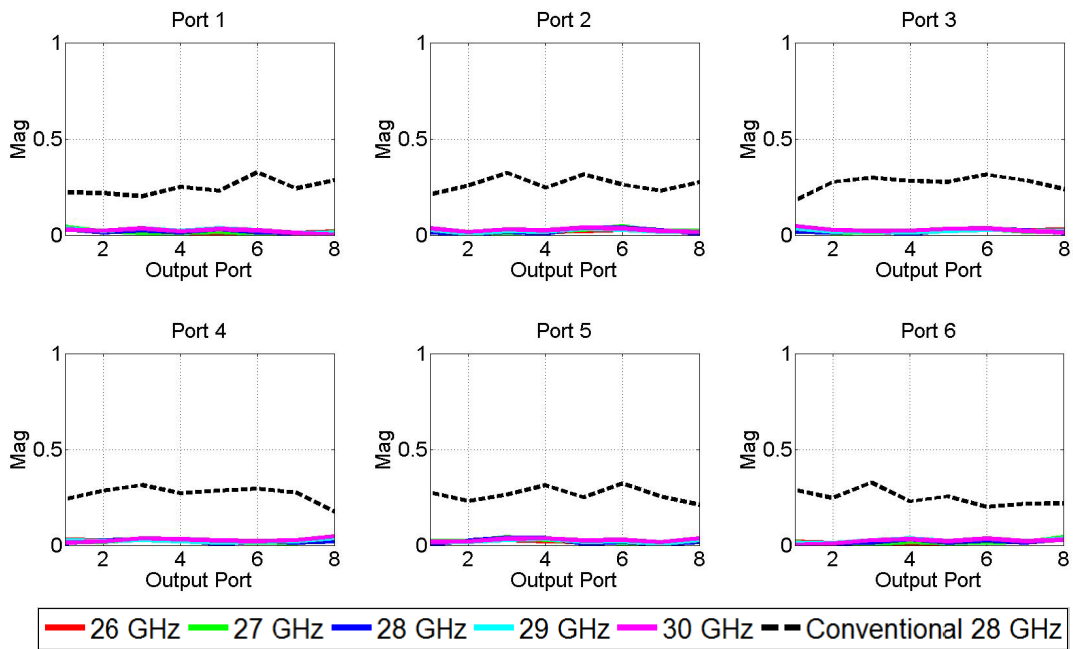


Figure 8. Magnitude performance of the conformal lens for case 2.

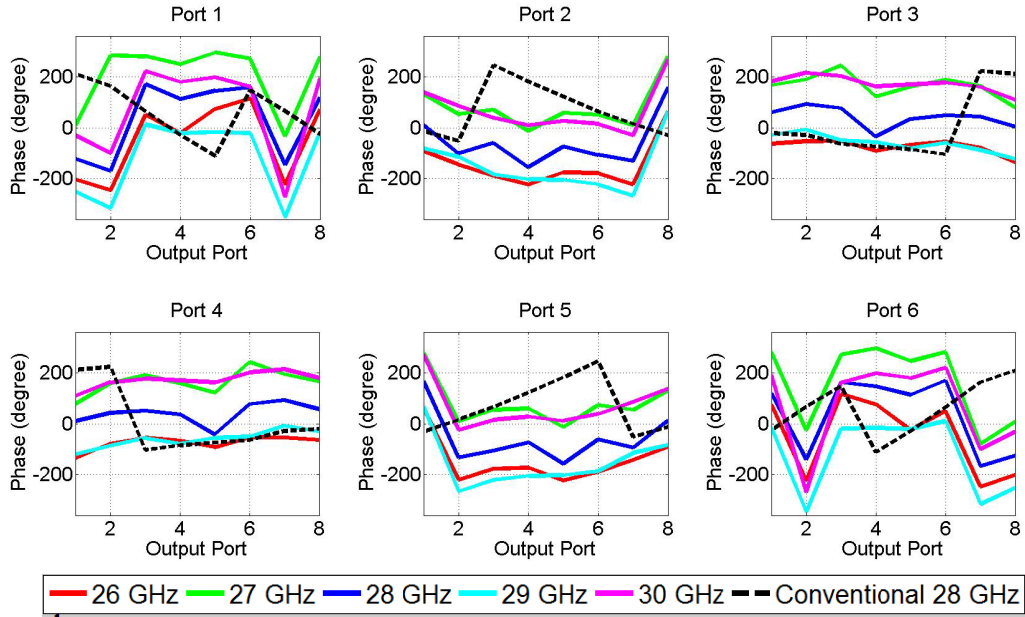


Figure 9. Phase performance of the conformal lens for case 2.

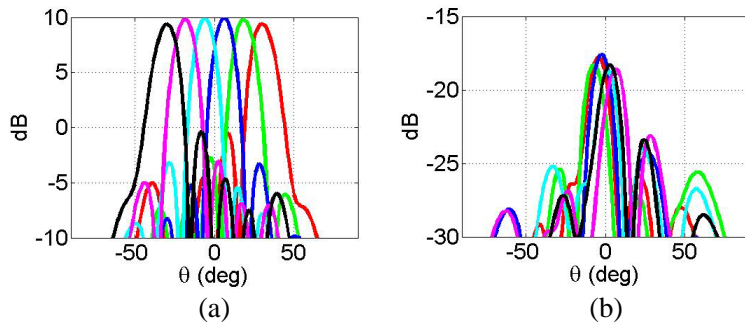


Figure 10. Radiation pattern of the (a) planar array, (b) conformal array fed by the lens in case 2 at 28 GHz.

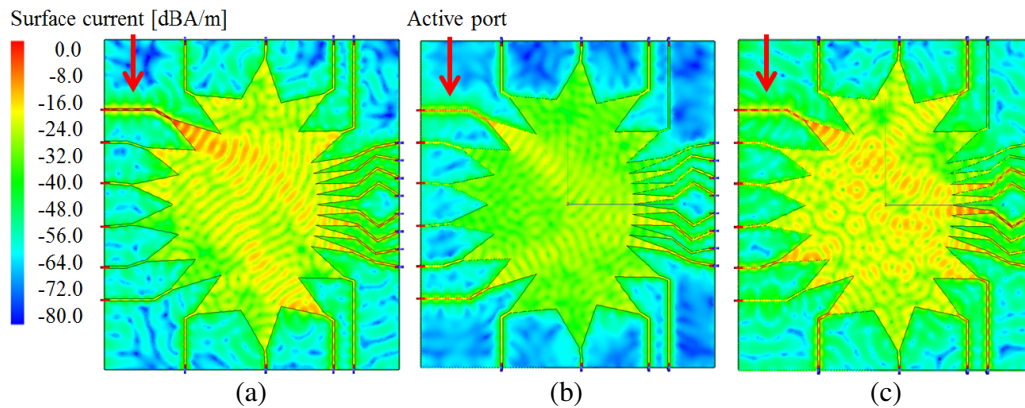


Figure 11. Surface currents with first port activated of (a) Conventional lens. (b) Conformal lens in case 1. (c) Conformal lens in case 2.

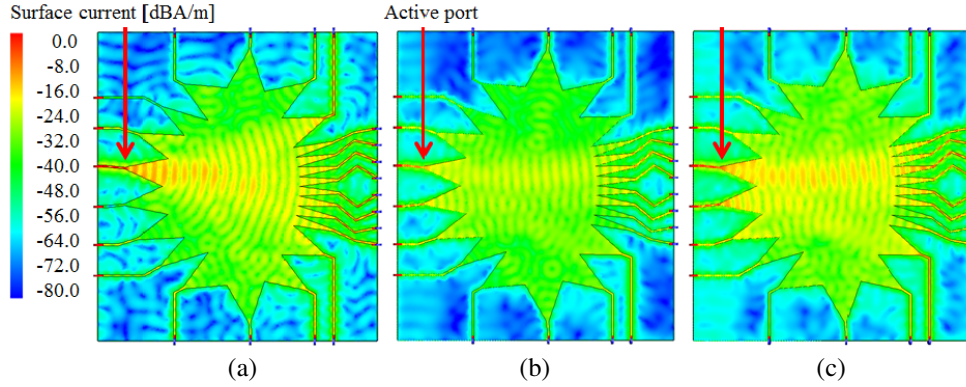


Figure 12. Surface currents with third port activated of (a) Conventional lens. (b) Conformal lens in case 1. (c) Conformal lens in case 2.

as the square of the radius of curvature of the bend. Fig. 11 shows the magnitude of current surfaces of the conventional lens, the conformal lenses in both Case 1 and Case 2 with the first input port is activated. It is obvious to see that there are some coupling effects near the dummy ports region of the conventional lens and these effects are absorbed by the dummy ports of the lens. Other than that, the conventional lens does not have significant reflection of current inside the dielectric slab. Fig. 11(b) shows the surface current of the conformal lens in case 1, compared with the conventional lens, the wave propagation from the input port is affected by the bent characteristic of the lens, which creates some reflection effects inside the structure. However, these reflection effects have low magnitude that they slightly change the phase performance of the conformal lens in case 1 compared with the conventional lens (as shown in Figs. 4 and 5). The most significant effect of reflection can be shown in Fig. 11(c) from the conformal lens in case 2, the reflection highly affects the wave propagation from the input port although some of them are absorbed by the dummy ports. The same effect happens when the third input ports of the lenses is activated as shown in Fig. 12. Therefore, Fig. 10 proves that when we feed the information from conformal lens of Case 2, the array antenna is not able to steer its main beam to desired directions, and the gain value of the array is decreased up to -15 dB.

3. CIRCULARLY FOLDED ROTMAN LENS

The idea of designing compact folded Rotman lens was implemented in [24, 25] using coupling vias as transitions between input ports (bottom layer) and output ports (top layer). However, the design of these lenses involve complicated steps including lens design with substrate integrated waveguide (SIW) technology, multiple branches coupling vias or short-circuited stubs waveguide optimization to maximize receive power at output ports [24]. This complexity makes the fabrication process difficult and expensive. Therefore, in this paper, we develop a folded model of a printed Rotman lens without any use of extra components such as coupling vias as in previous solutions. This idea was proposed in the conference paper [26] and is fully discussed in this paper. Fig. 13 demonstrates the use of our folded lens model inside a mobile phone. This configuration can support other types of devices with similar shapes such as smart watch, GPS devices, etc. Although the design of this lens involves in a circular bend, its fabrication process is not as difficult as it may appear. A conventional lens designed and fabricated on a thin substrate can be bent to conform to the surfaces discussed in this paper. This solution is simple and accurate as long as the substrate flexibility allows for the required bending. Another possible approach is to use the recent 3D-printing technology [31], which can offer a resolution up to $0.1 \mu\text{m}$. This would certainly be a costlier alternative but would provide a very accurate bend.

3.1. Design Procedure for Folded Lens

The two layers of the folded lens will be connected through a bent transition within the same substrate. Although it is shown in Section 2.2 that a conformal lens on a sharp curvature will malfunction due to

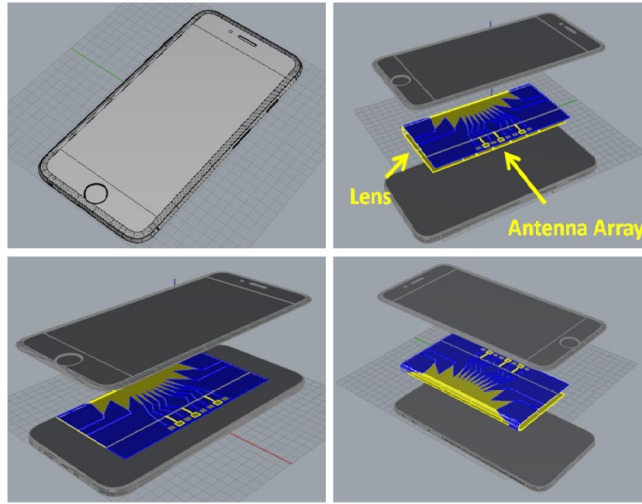


Figure 13. Folded lens concept integrated in a mobile phone.

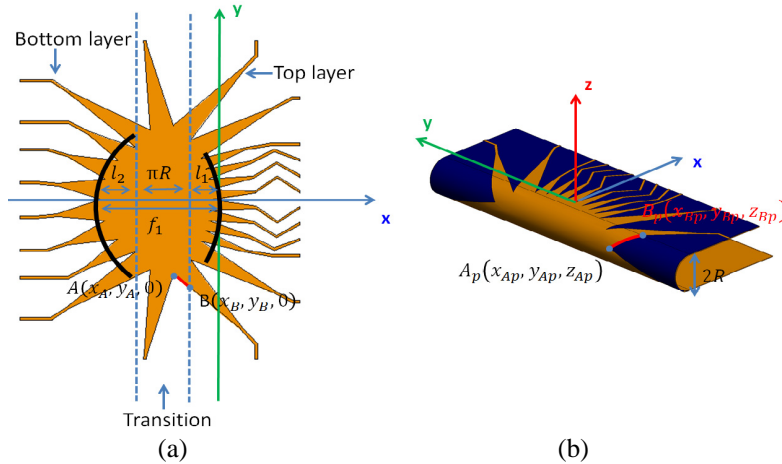


Figure 14. Design of folded Rotman lens. (a) Conventional lens. (b) Folded lens.

the bend in the feed lines, this is not the case for our proposed folded lens because the bend is created in the parallel plate region without any deformation of the feed line structures on both input and output ports of the lens. It can be shown in [30] that the E-plane bend will not affect the characteristics of wave propagating inside this region. Therefore, we do not anticipate the radius of the bend to have a significant effect on the performance of our folded lens design. It only affects the mechanical stability of the lens, as too small radii will not be practical.

As we observe, this folded design can reduce total lateral area of the lens by 50% with similar performance to a conventional Rotman lens with the same design parameters. Fig. 14 shows the design procedure and global coordinate system to design folded lens model. The folded lens will be used to support the uniform linear array antenna shown in Fig. 15.

We first identify three zones in the original structure of conventional Rotman lens (as shown in Fig. 14(a)) to achieve the folding. The first region, which is bounded from $(0, 0, 0)$ to $(-l_1, 0, 0)$, is used as the top layer of the folded lens. The second region ranging from $(-l_1, 0, 0)$ to $(-l_1 - \pi R, 0, 0)$ is the circular bent transition between the top layer and the bottom layer. Finally the bottom layer is defined by the region bounded from $(-l_1 - \pi R, 0, 0)$ to $(-l_1 - \pi R - l_2, 0, 0)$ where $l_2 = f_1 - (l_1 + \pi R)$. The dummy ports on the bent transition can be modeled by applying the 2 steps mentioned in Section 2.1 with some modifications. In the first step, by following the global coordinate system shown in Fig. 14(b),

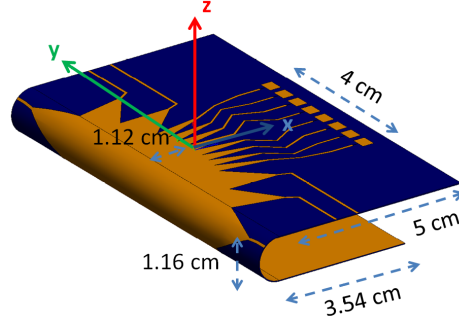


Figure 15. Design of folded Rotman lens.

the coordinate of projected points on the bending surface of the transition are calculated as (9) instead of (1).

$$x_{Ap} = -R \sin\left(\frac{|x_A + l_1|}{R}\right) - l_1, \quad y_{Ap} = y_A, \quad z_{Ap} = R \cos\left(\frac{|x_A + l_1|}{R}\right) - R \quad (9)$$

where (x_{Ap}, y_{Ap}, z_{Ap}) is the coordinate on the global coordinate system as shown in Fig. 14(b).

The second step is to apply the geodesics Equations (5)–(8) if the transition is chosen as cylindrical. If other types of transition are used such as parabolic or elliptical, the general geodesics equations in Equations (2)–(6) should be used depending on the type of transition. Similarly to the conformal lens design, the geodesics equation is applied on the local coordinate which has origin $O_{loc}(-l_1, 0, -R)$ and its unit vectors $\vec{x}_{loc} = \vec{x}$, $\vec{y}_{loc} = -\vec{z}$, and $\vec{z}_{loc} = \vec{y}$.

3.2. Simulation Results of Folded Lens

To verify the robustness of the folded lens idea, we design a folded lens operating at a center frequency of 28 GHz with parameters are specified in Table 2.

Table 2. Design parameters of circularly folded lens.

Design parameters	Folded lens
Bending radius (R)	0.58 cm
Focal length (f_1)	4.4 cm
Top layer length (l_1)	1.12 cm
Center frequency (f_0)	28 GHz
Ultralam 3850 (ϵ_r)	2.9
Substrate Thickness (h)	0.25 mm
Scanning range	-30° to 30°
Number of input	6
Number of output	8

Figure 15 shows the CAD model of the integrated system of the lens and the linear array antenna. Its magnitude and phase performance over the bandwidth from 26 GHz to 30 GHz is shown in Fig. 16 and Fig. 17, respectively. The performance of the conventional lens at center frequency of 28 GHz on planar structure with identical designed parameters is plotted in Fig. 16 and Fig. 17 for comparison. Fig. 18 shows the radiation pattern of the linear array on the same surface with the top layer of the lens that has patch elements designed at 28 GHz when it is fed by 6 input ports of the lens. We observe that the performance is very good compared to the conventional lens.

As mentioned above, the radius of the bending transition has no significant effect on the performance of the folded lens. In fact, as long as the substrate material is flexible enough, folded lens design can be designed with sharp bends to fit in compact spaces of electronic devices.

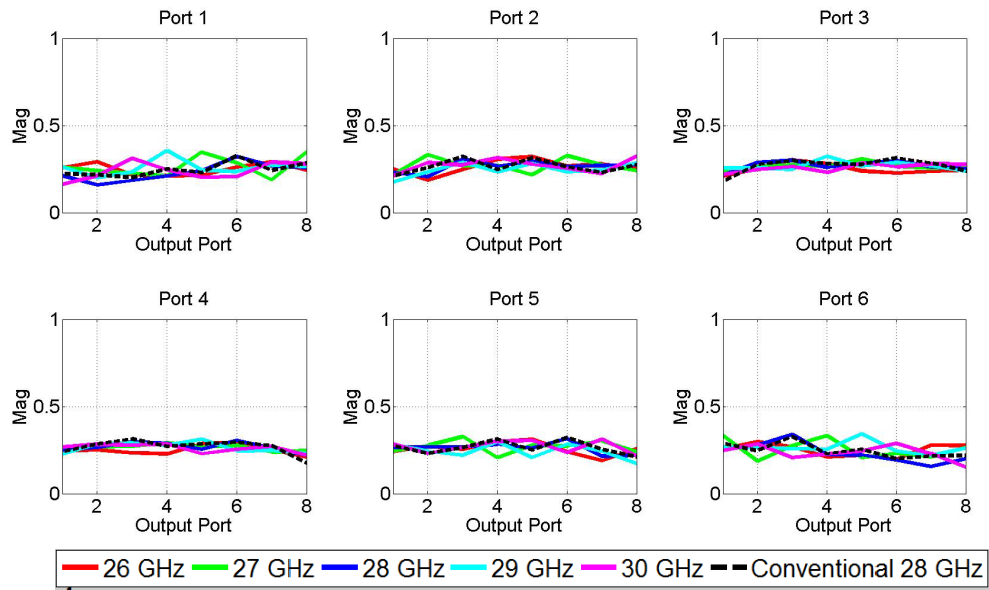


Figure 16. Magnitude performance of designed folded lens.

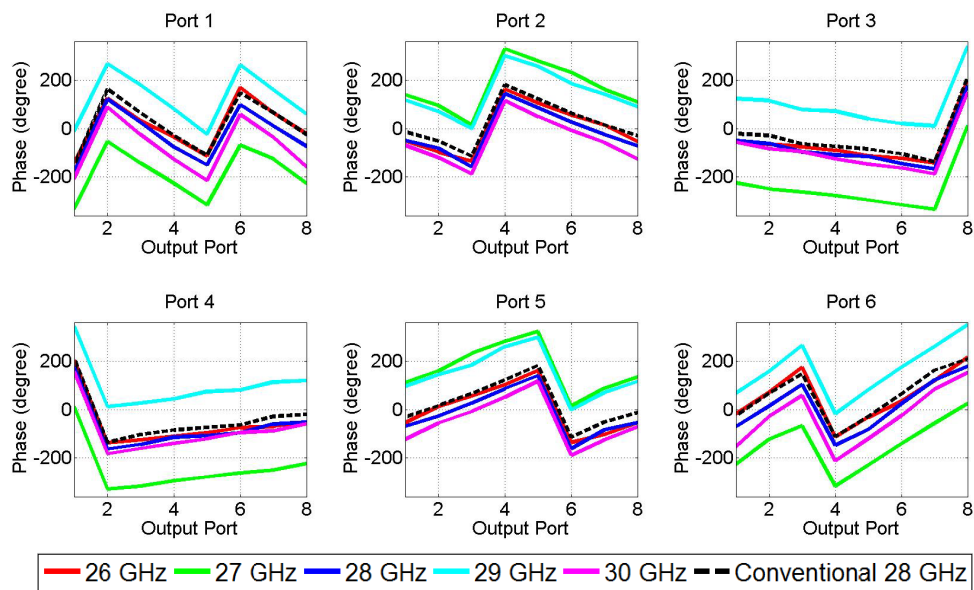


Figure 17. Phase performance of designed folded lens.

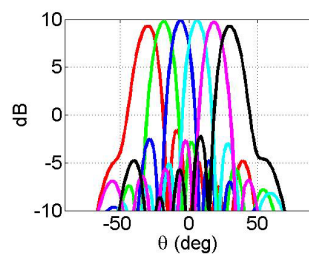


Figure 18. Radiation pattern at 28 GHz of the linear array fed by designed folded lens.

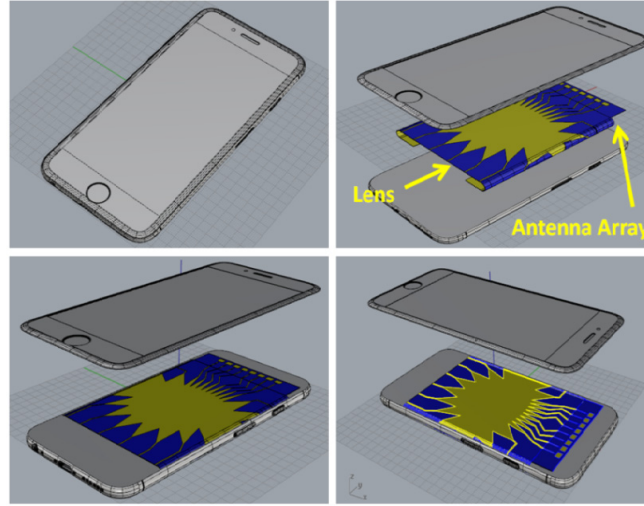


Figure 19. Wrapped lens integrated on the body of a mobile phone.

4. CIRCULARLY WRAPPED ROTMAN LENS

The wrapped lens employs a similar concept with the folded lens design by using a circular transition to connect the top and bottom layers of the lens. The difference between folded and wrapped configuration is that instead of creating the circular bent transition in the middle of the parallel plate region of the lens, we create the circular bend in the dummy port regions of the lens to reduce the overall dimensions of this region. This wrapped configuration is also suitable to be integrated into mobile phone or any similar shaped devices as demonstrated in Fig. 19. In the wrapped lens configuration, since only the structure of dummy port is bent, the true time delay performance of wrapped lens should be similar to its original lens performance. As observe, the designed wrapped lens configuration has similar performance with conventional lens structure with total lateral area are reduced up to 50%.

4.1. Design Procedure of Wrapped Lens

The design of wrapped lens is similar to the folded lens by following two main procedures. The global coordinate system is chosen as in Fig. 20(b) and the design procedure is shown as follows.

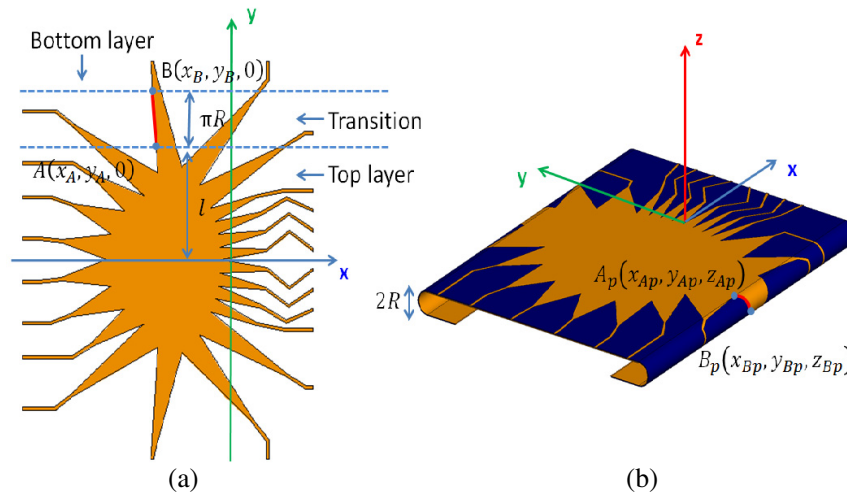


Figure 20. Design of wrapped Rotman lens. (a) Conventional lens. (b) Wrapped lens.

We first divide the conventional Rotman lens (as shown in Fig. 20(a)) into 3 regions. The first region, which extends from $(0, 0, 0)$ to $(0, l, 0)$, is used as the top layer of the wrapped lens. The second region bounded from $(0, l, 0)$ to $(0, l + \pi R, 0)$, is the transition between the top layer and the bottom layer. Finally the bottom layer is defined by the region bounded from $(0, l + \pi R, 0)$ to $(0, y_{\max}, 0)$ where y_{\max} is the maximum y -coordinate of the original lens region. With the global coordinate system shown in Fig. 20(b), the coordinate of projected points on the bending surface of the transition are calculated as Eq. (10).

$$x_{Ap} = x_A, \quad y_{Ap} = R \sin\left(\frac{|y_A - l_1|}{R}\right) + l_1, \quad z_{Ap} = R \cos\left(\frac{|y_A - l_1|}{R}\right) - R \quad (10)$$

where (x_{Ap}, y_{Ap}, z_{Ap}) is the coordinate on the global coordinate system as shown in Fig. 20(b).

Similar to the folded lens design, the second step is to apply the geodesics Equations (5)–(8) if the transition is chosen as cylindrical. If other types of transition are used such as parabolic or elliptical, the general geodesics Equations in (2)–(6) should be used depending on the type of transition. Also, the geodesics equation is applied on the local coordinate which has origin $O_{loc}(0, l, -R)$ and its unit vectors $\vec{x}_{loc} = -\vec{z}$, $\vec{y}_{loc} = \vec{y}$, and $\vec{z}_{loc} = \vec{x}$.

4.2. Simulation Results of Wrapped Lens

To verify its performance, we designed a wrapped lens operating at a center frequency of 28 GHz with parameters specified in Table 3.

Table 3. Design parameters of circularly wrapped lens.

Design parameters	Wrapped lens
Bending radius (R)	0.3 cm
Focal length (f_1)	4.4 cm
Top layer length (l)	3.2 cm
Center frequency (f_0)	28 GHz
Ultralam 3850 (ϵ_r)	2.9
Substrate Thickness (h)	0.25 mm
Scanning range	-30° to 30°
Number of input	6
Number of output	8

Figure 21 shows the CAD model of the integrated system of the lens with the linear array antenna. Its magnitude and phase performance over the bandwidth from 26 GHz to 30 GHz is shown in Fig. 22 and Fig. 23, respectively. The performance of the conventional lens at center frequency of 28 GHz on planar structure with identical designed parameters is plotted in Fig. 22 and Fig. 23 for a comparison. Fig. 24 shows the radiation pattern of the linear array fed by 6 input ports of the lens.

Since we are interested in practical devices that are commercially available, we adopted the dimensions and designed the wrapped lens so that it fits inside an iPhone 6s. This explains why the bending radius of the wrapped lens is small. Our simulation results in Figs. 22–24 show that the wrapped lens performs very well and similar to the conventional lens performance. Since the original dimensions of the conventional lens are $10 \text{ cm} \times 11 \text{ cm}$ and the dimensions of the wrapped lens are $6.4 \text{ cm} \times 11 \text{ cm}$, the design wrapped lens dimensions are reduced about 40% of the original dimensions. We can potentially further reduce the width dimensions of the lens by up to 50% by optimizing the dummy port region.

The radiation pattern produced by the linear array antenna shown in Fig. 21 fed by magnitude and phase from all output ports of the wrapped lens has acceptable gain value at about 10 dB with side lobe level about -4 dB .

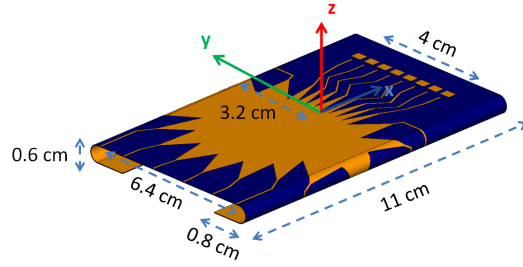


Figure 21. Design of wrapped Rotman lens.

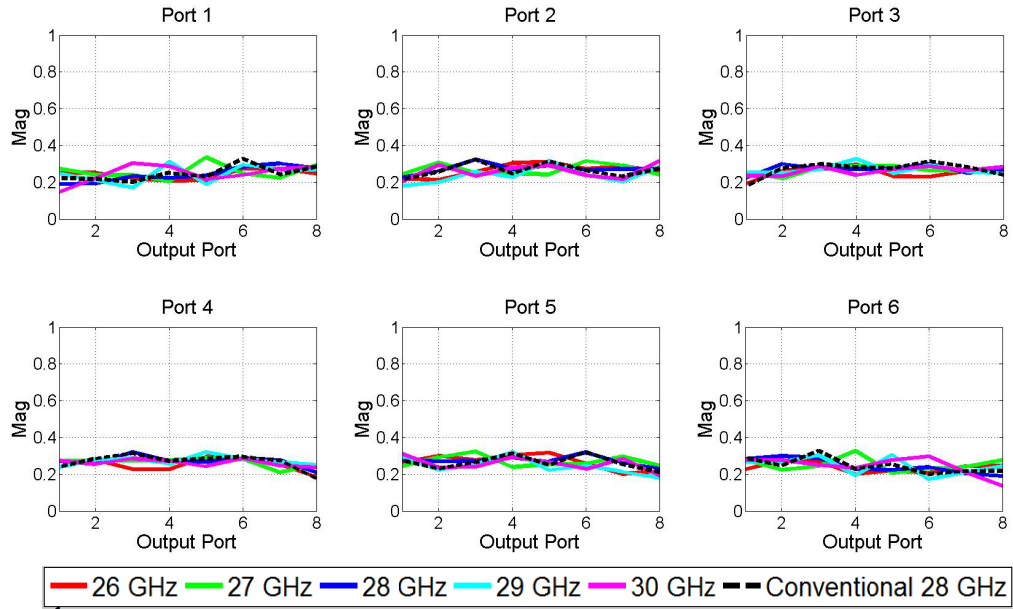


Figure 22. Magnitude performance of designed wrapped lens.

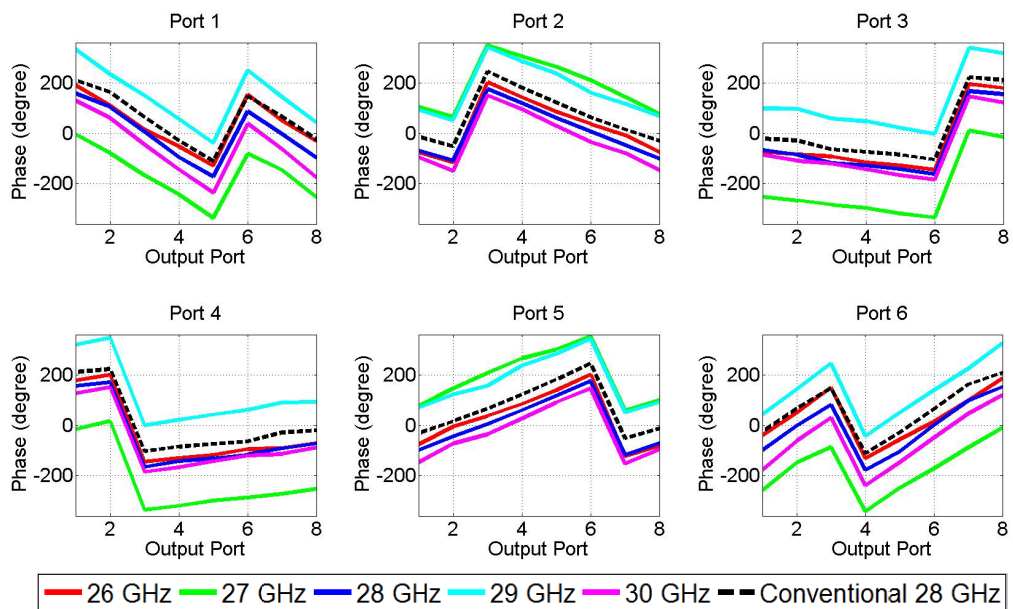


Figure 23. Phase performance of designed wrapped lens.

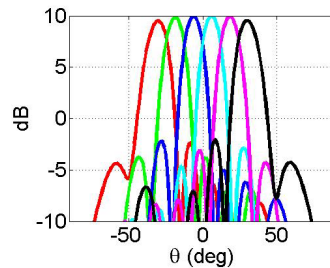


Figure 24. Radiation pattern at 28 GHz of the linear array fed by designed wrapped lens.

5. CONCLUSION

In this work, we investigate the idea of modifying the planar structure of Rotman lens into different configurations such as conformal lens, folded lens, and wrapped lens. These modified structures can be integrated into modern devices such as curved TV, smart watch, mobile phone, etc. to support millimeter wave technology for cellular communication. The applicability of conformal lens is shown using a cylindrical curvature, but the method applies to other curvatures as well. Similarly, the folded lens and wrapped lens design are shown using a circular bent transition to connect the top layer with the bottom layer of the lens, but it can be designed with parabolic or elliptical curvature. The results show that these modified configurations of conformal lens, folded lens, and wrapped lens have similar performance to conventional Rotman lens. However, the folded lens and wrapped lens design can reduce the total dimensions of the lens by 50% that can be used for integration in embedded or compact transceiver system.

REFERENCES

1. Rotman, W. and R. Turner, "Wide-angle microwave lens for line source applications," *IEEE Transactions on Antennas and Propagation*, Vol. 11, 623–632, 1963.
2. Smith, M. S., "Design considerations for Ruze and Rotman lenses," *Radio and Electronic Engineer*, Vol. 52, No. 4, 181–187, 1982.
3. Smith, M. S. and A. K. S. Fong, "Amplitude performance of Ruze and Rotman lenses," *Radio and Electronic Engineer*, Vol. 53, No. 9, 329–336, 1983.
4. Hansen, R. C., "Design trades for Rotman lenses," *IEEE Transactions on Antennas and Propagation*, Vol. 39, No. 4, 464–472, 1991.
5. Katagi, T., S. Mano, S. Sato, S. Tahara, and E. Tomimatsu, "An improved design method of Rotman lens antennas," *IEEE Antennas and Propagation Society International Symposium*, Vol. 20, 136–139, 1982.
6. Weiss, S. and O. Kilic, "Rotman lens design for aperiodic arrays," *Pro. IEEE AP-S/URSI Intl. Conference*, Toronto, Canada, July 2010.
7. Weiss, S., A. Zaghoul, and O. Kilic, "Measurement and simulation of Rotman lens designs that mitigate internal diffraction effects," *Proc. IEEE AP-S/URSI Intl Conference*, Toronto, Canada, July 2010.
8. Nguyen, T., T. K. Vo Dai, and O. Kilic, "Rotman lens-fed aperture coupled array antenna at millimeter wave," *IEEE APS/URSI 2016*, Fajardo, Puerto Rico, USA, July 2016.
9. Rappaport, C. and A. Zaghoul, "Optimized three-dimensional lenses for wide-angle scanning," *IEEE Transactions on Antennas and Propagation*, Vol. 33, No. 11, 1227–1236, 1985.
10. Dong, J., A. I. Zaghoul, and R. Rotman, "Phase-error performance of multi-focal and non-focal two-dimensional Rotman lens designs," *IET Microwaves, Antennas & Propagation*, Vol. 4, No. 12, 2097–2103, 2010.
11. Vo Dai, T. K. and O. Kilic, "A non-focal rotman lens design to support cylindrically conformal array antenna," *The Applied Computational Electromagnetics Society Express Journal*, Vol. 7, July 2016.

12. Kilic, O. and R. Dahlstrom, "Rotman lens beam formers for Army multifunction RF antenna applications," *2005 IEEE Antennas and Propagation Society International Symposium*, Vol. 2, 2005.
13. Kilic, O. and S. Weiss, "Rotman lens designs for military applications," *Radio Science Bulletin*, No. 333, 10–24, 2010.
14. Zaghoul, A., O. Kilic, S. Weiss, and E. Adler, "Realization of Rotman's concepts of beamformer lenses and artificial dielectric materials," *IEEE International Conference on Microwaves, Communications, Antennas and Electronics Systems, COMCAS 2009*, 2009.
15. Weiss, S., S. Keller, and C. Ly, "Development of simple affordable beamformers for army platforms," *Proceedings of GOMACTech — 07 Conference*, Lake Buena Vista, FL, 2006.
16. Schulwitz, L. and A. Mortazawi, "A new low loss Rotman lens design using a graded dielectric substrate," *IEEE Transactions on Microwave Theory and Techniques*, Vol. 56, No. 12, 2734–2741, 2008.
17. Hirokawa, J. and M. Ando, "Single-layer feed waveguide consisting of posts for plane TEM wave excitation in parallel plates," *IEEE Transactions on Antennas and Propagation*, Vol. 46, No. 5, 1998. 625–630.
18. Cheng, Y. J., W. Hong, K. Wu, Z. Q. Kuai, C. Yu, J. X. Chen, J. Y. Zhou, and H. J. Tang, "Substrate integrated waveguide (SIW) Rotman lens and its Ka-band multibeam array antenna applications," *IEEE Transactions on Antennas and Propagation*, Vol. 56, No. 8, 2504–2513, 2008.
19. Peterson, A. F. and E. O. Rausch, "Scattering matrix integral equation analysis for the design of a waveguide Rotman lens," *IEEE Transactions on Antennas and Propagation*, Vol. 47, No. 5, 870–878, 1999.
20. Gandini, E., M. Ettorre, M. Casaletti, K. Tekkouk, L. Le Coq, and R. Sauleau, "SIW slotted waveguide array with pillbox transition for mechanical beam scanning," *IEEE Antennas and Wireless Propagation Letters*, Vol. 11, 1572–1575, 2012.
21. Casaletti, M., R. Sauleau, M. Ettorre, and S. Maci, "Efficient analysis of metallic and dielectric posts in parallel-plate waveguide structures," *IEEE Transactions on Microwave Theory and Techniques*, Vol. 60, No. 10, 2979–2989, 2012.
22. Casaletti, M., G. Valerio, J. Seljan, M. Ettorre, and R. Sauleau, "A full-wave hybrid method for the analysis of multilayered SIW-based antennas," *IEEE Transactions on Antennas and Propagation*, Vol. 61, No. 11, 5575–5588, 2013.
23. Ettorre, M., R. Sauleau, and L. Le Coq, "Multi-Beam multi-layer leaky-wave SIW pillbox antenna for millimeter-wave applications," *IEEE Transactions on Antennas and Propagation*, Vol. 59, No. 4, 1093–1100, 2011.
24. Tekkouk, K., et al., "Multibeam SIW slotted waveguide antenna system fed by a compact dual-layer Rotman lens," *IEEE Transactions on Antennas and Propagation*, Vol. 64, No. 2, 504–514, 2016.
25. Tudosie, G. and R. Vahldieck, "An LTCC-based folded Rotman lens for phased array applications," *2006 Asia-Pacific Microwave Conference*, 2006.
26. Vo Dai, T. K. and O. Kilic, "Designing folded Rotman lens," *IEEE International Symposium on Antennas and Propagation/USNC-URSI National Radio Science Meeting*, 2016.
27. Josefsson, L. and P. Persson, *Conformal Array Antenna Theory and Design*, Vol. 29, John Wiley & Sons, 2006.
28. Jha, R. M., S. A. Bokhari, V. Sudhakar, and P. R. Mahapatra, "Closed form expressions for integral ray geometric parameters for wave propagation on general quadric cylinders," *Antennas and Propagation Society International Symposium, 1989. AP-S. Digest*, 203–206, 1989.
29. Rice, S. O., "Reflections from circular bends in rectangular wave guides — Matrix theory," *Bell System Technical Journal*, Vol. 27, No. 2, 305–349, 1948.
30. Barlow, H. E. M., "Propagation around bends in waveguides," *Proceedings of the IEE-Part C: Monographs*, Vol. 106, No. 9, 11–15, 1959.
31. nScript, Inc., <http://nscript.com/>, October 2016.